Heteromaterial-gate line tunnel field-effect transistor based on Si/Ge heterojunction*

Shuqin Zhang(张书琴), Renrong Liang(梁仁荣)†, Jing Wang(王敬), Zhen Tan(谭桢), and Jun Xu(许军)

Tsinghua National Laboratory for Information Science and Technology Institute of Microelectronics, Tsinghua University, Beijing 100084, *China*

(Received 22 June 2016; revised manuscript received 21 October 2016; published online 22 December 2016)

A Si/Ge heterojunction line tunnel field-effect transistor (LTFET) with a symmetric heteromaterial gate is proposed. Compared to single-material-gate LTFETs, the heteromaterial gate LTFET shows an off-state leakage current that is three orders of magnitude lower, and steeper subthreshold characteristics, without degradation in the on-state current. We reveal that these improvements are due to the induced local potential barrier, which arises from the energy-band profile modulation effect. Based on this novel structure, the impacts of the physical parameters of the gap region between the pocket and the drain, including the work-function mismatch between the pocket gate and the gap gate, the type of dopant, and the doping concentration, on the device performance are investigated. Simulation and theoretical calculation results indicate that the gap gate material and n-type doping level in the gap region should be optimized simultaneously to make this region fully depleted for further suppression of the off-state leakage current.

Keywords: line tunnel field-effect transistor, heteromaterial gate, fully depleted

PACS: 85.30.–z, 85.30.Mn, 85.35.–p **DOI:** 10.1088/1674-1056/26/1/018504

1. Introduction

As the feature size is being scaled down, metal-oxide-semiconductor field-effect transistors (MOSFETs) are facing serious problems. The short-channel effects are one of the most intractable challenges. Because of thermodynamic restrictions, the subthreshold swing (SS) of MOSFET devices must have a minimum value of 60 mV/dec at room temperature. This causes high power dissipation. Tunnel field-effect transistors (TFETs) have been attracting much attention because of their new operating mechanism. The TFETs are driven by band-to-band tunnelling (BTBT), and their SS values are no longer limited to 60 mV/dec; thus, the power consumption can be reduced greatly.[1–5] However, the BTBT mechanism inevitably causes the on-state current of TFETs to be lower than that of MOSFETs by approximately two to four orders of magnitude, limiting the applications of TFETs.[6–11] In addition, contrary to the theoretical prediction, it has been shown experimentally that the SS values of many fabricated TFET devices are much higher than 60 mV/dec.[12–14] Therefore, new channel materials and innovative device structures, such as narrow band-gap materials,[15–17] green FETs,[18] multi-gate TFETs,[19–21] and line TFETs (LTFETs)[22] have been developed to overcome the shortcomings of the TFETs. On one hand, compared to bare Si TFETs, the Ge- and SiGe-channel TFETs have been verified to be potential candidates because of the higher tunnelling rates resulting from the narrow band gaps of Ge.[23–27] On the other hand, many investigations have shown that the LTFETs perform well in terms of the on-state current because of the enlarged tunnelling area.[28–30] However, both suffer from relatively large off-state leakage currents, which degenerate the on/off current ratio. Previously, a heteromaterial-gate (HMG) structure had been proposed and applied to the design of point TFETs to improve their device performance by energy-band profile modulation.[31,32] Few studies have also reported the implementation of the HMG configuration in LTFETs.

In this work, a novel Si/Ge heterojunction LTFET device combined with a symmetric HMG structure is proposed and investigated through two-dimensional (2D) numerical simulations. The results show that the HMG LTFET has much lower off-state currents and superior subthreshold characteristics compared to the traditional single-material-gate (SMG) LTFETs. The lateral energy-band modulation effect induced by the HMG is examined in detail. The work-function mismatch of the HMG has significant impacts on the off-state leakage current and subthreshold characteristics, because of the modulation of the degree of depletion in the gap region. To achieve better performance, the dopant type and doping concentration in this region are also optimized considering the theoretical calculations for the width of the depletion layer. All numerical simulations are carried out using Sentaurus TCAD (Synopsys, San Jose, CA).[33]

*Project supported by the National Natural Science Foundation of China (Grant No. 61306105), the National Science and Technology Major Project of China (Grant No. 2011ZX02708-002), the Tsinghua University Initiative Scientific Research Program and the Tsinghua National Laboratory for Information Science and Technology (TNList) Cross-discipline Foundation of China.

†Corresponding author. E-mail: liangrr@mail.tsinghua.edu.cn

2. Device structure

Figures 1(a) and 1(b) show the cross-sectional views of a conventional SMG LTFET and the proposed HMG LTFET, respectively. The source/pocket junction is the main region where vertical BTBT occurs in the on state, and the gap region connects the pocket and drain regions. The lengths of the pocket and gap regions are 20 nm and 5 nm, respectively, and both are 5 nm thick. The source is B-doped (10^{19} cm^{-3}) Ge. The pocket, gap, and drain regions are all abrupt P-doped Si with doping concentrations of 10^{17} cm^{-3}, 10^{15} cm^{-3}, and 10^{20} cm^{-3}, respectively. The metal gate of the proposed HMG LTFET is composed of one pocket gate and two symmetrical gap gates; the pocket gate in the pocket region is M1 with a fixed work function of φ_1, and the gap gate in the gap region is M2 with a tuneable work function of φ_2. Hence, the proposed HMG LTFET is equivalent to a series connection of a vertical tunnelling junction controlled by M1 and a lateral n-type junctionless transistor (JLT) gated by M2.[34] HfO_2 with a thickness of 2 nm serves as the gate oxide. The main physical model used to describe the operating principle of this proposed LTFET in the simulation is the dynamic non-local BTBT model, which offers an analytical expression for the tunnelling rate using the Kane model[33]

$$R_{\text{net}} = A\left(\frac{F}{F_0}\right)^P \exp\left(-\frac{B}{F}\right), \tag{1}$$

where R_{net} is the electron BTBT generation rate in a uniform electric field. F represents the electric field with a default value F_0 of 1 V·cm^{-1}. P is 2.5 for indirect tunnelling. A and B are variables given by $A = 1.46 \times 10^{17}$ cm^{-3}·s^{-1} and $B = 3.59 \times 10^6$ V·cm^{-1} in this work, as calibrated using previous experimental data.[35] In addition, the Shockley–Read–Hall (SRH) and Auger recombinations are involved. In view of the high doping concentrations in the drain regions, the band-gap narrowing model and the Fermi statistics are also employed. The lateral transport of the carriers is described by the doping-dependent mobility model.

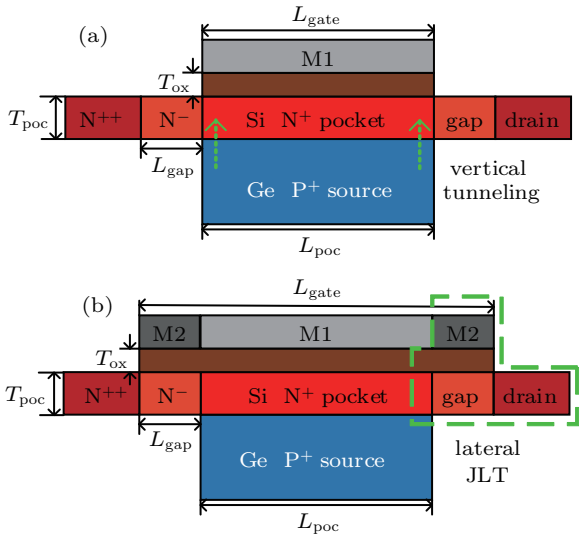

Fig. 1. (color online) Schematic structures of (a) conventional single-material-gate (SMG) line TFET (LTFET) and (b) proposed heteromaterial-gate (HMG) LTFET based on a Si/Ge heterojunction. The channel of the HMG LTFET consists of three parts: the pocket region above the source and the two gap regions connecting the pocket and drain regions. The pocket gate and gap gate are named M1 and M2. The green dashed box shows the equivalent lateral n-type junctionless transistor (JLT) gated by M2.

3. Results and discussion

The transfer characteristics of our proposed HMG LTFET are compared with those of the SMG LTFETs at $V_{\text{ds}} = 0.6$ V, in Fig. 2. The gate work function of the SMG LTFET was set to two different values of 4.1 eV and 4.5 eV, which were the values of φ_1 and φ_2 of the HMG LTFET. As expected, the shapes of the two I_{ds}–V_{gs} curves were mostly identical for the SMG devices. The difference in the gate work functions was evident only in the shift in the onset voltage, which was marked as V_{off},[31] indicating the switching of the transistor from the off state to the on state. However, for the HMG LTFET, the introduction of the HMG configuration made a big difference, achieving several advantages simultaneously: the off-state leakage current was lower by approximately three orders of magnitude, the SS was smaller, and no degradation was observed in the on-state current. The inset shows the point SS, which can be calculated as $\mathrm{d}V_{\text{gs}}/\mathrm{d}(\lg I_{\text{ds}})$ and which varies with the increasing drain current. It can be seen that the proposed HMG LTFET has the minimum point SS at approximately 10 mV/dec.

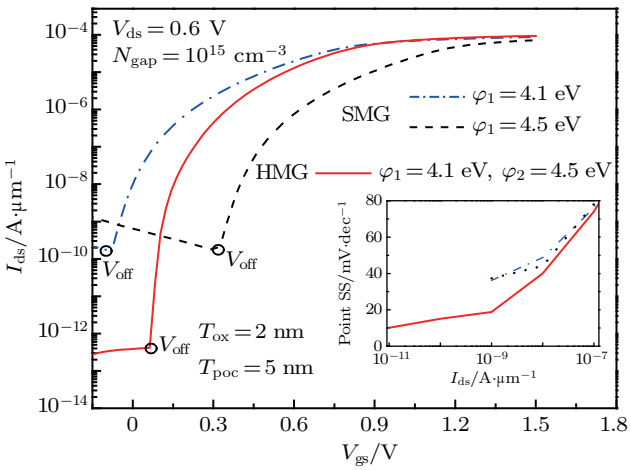

Fig. 2. (color online) Transfer characteristics of SMG and HMG LTFETs at $V_{\text{ds}} = 0.6$ V. The latter shows the superior properties of lower off-state leakage current and steeper subthreshold slope. The inset displays the values of the point SS as a function of drain current.

The enhanced performance can be explained further by the change in the energy band diagram of the HMG LTFET in Fig. 3. V_{ds} was maintained at 0.6 V and V_{gs} was assigned several values to represent the different operating modes of the device. When $V_{\text{gs}} = -0.1$ V, both the SMG and HMG LTFETs

were in the off state and the drain leakage current was primarily from the lateral electron drift–diffusion. However, the work function of the gap gate, φ_2, was higher than that of the pocket gate, φ_1, which pulled up the energy band in the gap region, resulting in a maximum conduction band (E_c). Thus, a local electron potential barrier was formed, leading to a significant reduction in the off-state leakage current.

When a positive V_{gs} larger than V_{off} was applied to the gate, the two SMG LTFETs and the HMG LTFET were in the on state. The vertical tunnelling from the source to the pocket was dominant, and the tunnelling direction was perpendicular to the surface plane of the gate oxide. Because the energy band in the vertical direction was controlled by M1, the SMG and HMG LTFETs with $\varphi_1 = 4.1$ eV had similar band profiles in this direction. Therefore, the difference in their drain currents was mainly caused by the modulated lateral JLT. The effect of the applied positive V_{gs} on the energy band contends with that of the higher work function of the gap gate. When the positive V_{gs} is relatively low (e.g., $V_{gs} = 0.6$ V), the raising of the energy band induced by the gap gate is dominant; therefore, the conduction band of the HMG device will be higher than that of the SMG device. However, when V_{gs} is high enough (e.g., $V_{gs} = 1.5$ V, as shown in Fig. 3), the energy band of HMG LTFETs would be pushed down to a level lower than that of the SMG devices. In this case, the drain current of the HMG LTFET can surpass that of the SMG LTFET, with increase in V_{gs}.

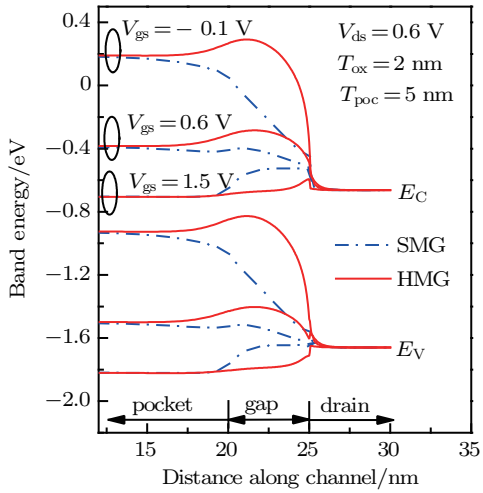

Fig. 3. (color online) Energy band diagram along a horizontal cutline for SMG ($\varphi_1 = 4.1$ eV) and HMG LTFETs ($\varphi_1 = 4.1$ eV, $\varphi_2 = 4.5$ eV) at $V_{gs} = -0.1$ V, 0.6 V, and 1.5 V. The cutline is 0.5 nm below the interface between the gate oxide and the Si channel.

To gain insight into the dependence of the work-function mismatch, a HMG LTFET with different gap-gate work functions is also studied, and the transfer characteristics are presented in Fig. 4(a). In the simulations, the values of φ_2 are varied from 3.7 eV to 4.7 eV in increments of 0.2 eV, while φ_1 is kept unchanged at 4.1 eV. The simulated results show that this variable has a remarkable influence on the performance of the HMG device. It can be seen intuitively that a lower work function of the gap gate causes deterioration in the SS_{ave} and I_{off}. Here, SS_{ave} is defined as the average subthreshold swing, which can be expressed as:[36]

$$SS_{ave} = \frac{V_t - V_{off}}{\log I_t - \log I_{off}}, \tag{2}$$

where I_{off} is extracted as the drain current at $V_{gs} = V_{off}$. V_t is defined as the gate voltage at which the drain current $I_t = 10^{-7}$ A/μm.

On one hand, when φ_2 was less than φ_1, the smaller φ_2 led to a lower energy band in the gap region; thus, a lower barrier height for electrons for drift–diffusion could cause a higher I_{off}. However, this reduction in the band energy was favourable for boosting the drain current in the on state. Under a positive gate voltage, the lateral JLT was turned on. In this case, this JLT played the role of a series resistor, whose value was primarily adjusted by M2. The electron density in the surface of this region became larger as φ_2 decreased, making this region a relatively lower resistance channel, and the on-state current was enhanced. Nevertheless, the discrepancy in the on-state current was very slight as V_{gs} increased. On the other hand, if $\varphi 2$ was larger than φ_1, the lateral JLT was in the off state under negative V_{gs}, and the leakage current was generated at the bottom of the channel, i.e., the gap region. In this case, the gap region was depleted and the width of the depletion layer increased as φ_2 increased. Therefore, there was a minimum I_{off} when the gap region became fully depleted with a critical value of φ_2, and it could not be reduced further even when a higher φ_2 was adopted. In addition, the excessive increase in φ_2 was detrimental to the on-state current because of the lateral local potential barrier that was formed.

Figure 4(b) shows the SS_{ave} and I_{on}/I_{off} ratio as functions of φ_2 for the simulated HMG LTFETs. I_{on} was extracted as the drain current at $V_{gs} - V_{off} = 0.6$ V and $V_{ds} = 0.6$ V. Both of them change significantly when φ_2 is lower than 4.3 eV. The I_{on}/I_{off} ratio increases and SS_{ave} decreases because of the decreasing I_{off}. However, both of them change in an opposite manner when φ_2 is increased further, which is because I_{off}tends to saturate whereas I_{on} reduces.

In addition to the work-function mismatch, the dopants in the gap region were also predicted to influence the performance of the HMG LTFET. It needs to be pointed out that the thicknesses of the gate oxide and gap region also have impacts on the device characteristics. The former affects the capability of gate control over the channel and the latter determines the leakage current in the off state. In this section, we modify these two parameters to further highlight the modulation effect of the gap gate on the gap region. The transfer characteristics with various dopant types and doping concentrations

in the gap region of the HMG LTFET with a 3-nm-thick gap region and a 1-nm-thick gate oxide are depicted in Fig. 5(a). Because the same structure is used for the pocket region and the gate stack on top of it, the onset voltage and on-state current of all simulated devices are almost the same. The obvious difference is reflected in the off state, which depends primarily on the gap region. The HMG LTFETs with an n-type gap have a flat ambipolar window in a certain range of negative gate voltages, while those with a p-type gap transform immediately from forward operation to an ambipolar state. The inset shows the simulated hole current density of an HMG LTFET with a p-type (10^{18} cm^{-3}) gap region at $V_{gs} = -0.1$ V. In this case, the p-type gap was accumulated and the hole drift–diffusion current was collected in the source region. As V_{gs} became more negative, a hole BTBT process from the drain to the gap region was induced by the higher energy band in the gap region, which also contributed to the ambipolar current. This caused the I_{ds}–V_{gs} curves of the HMG LTFET devices with a p-type gap to appear in the form of a 'V'.

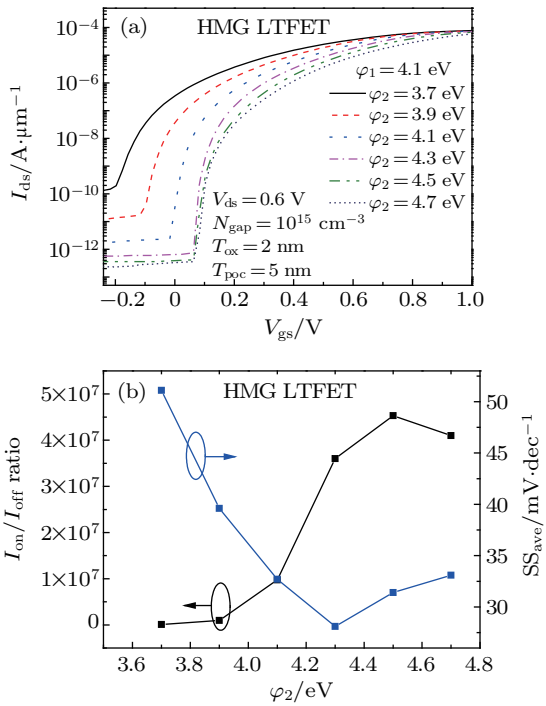

Fig. 4. (color online) (a) Simulated I_{ds}–V_{gs} characteristics of the HMG LTFET, showing their dependence on various work functions of the gap gate at $V_{ds} = 0.6$ V. (b) φ_2 dependence of SS_{ave} and I_{on}/I_{off} ratio extracted from these simulated devices.

For transistors with an n-type gap, it was noticeable that a relatively low doping level varying from 10^{15} cm^{-3} to 10^{18} cm^{-3} caused almost no difference in the off-state current. However, when the doping level was changed from 10^{19} cm^{-3} to 10^{20} cm^{-3}, the off-state current increased dramatically, as can be observed in Fig. 5(b). Because V_{off} was larger than zero, the n-type gap region was in a depleted state under the low negative V_{gs}, and the width of the depletion layer decreased with increasing doping concentration. Figure 5(c) presents a comparison of the electron current densities for the gap region with n-type doping of 10^{18} cm^{-3}and 10^{20} cm^{-3} at $V_{gs} = -0.1$ V. The distributions of electron current clearly show that the gap region is fully depleted with a relatively low doping level and that it becomes partially depleted as the doping level becomes sufficiently high.

To quantitatively estimate the width of the depletion layer, we use the depletion approximation. The gate voltage equation for the lateral JLT can be expressed as follows:

$$V_{gs} - V_{fb} = \varphi_s - \frac{t_{ox}}{\varepsilon_{ox}}\sqrt{2\varepsilon_{Si} q N_{gap} |\varphi_s|}, \tag{3}$$

where q is the charge of the electron, φ_s is the surface potential, and t_{ox} is the thickness of the gate oxide layer. ε_{ox} and ε_{Si} are the dielectric constants of the gate oxide and Si, respectively. N_{gap} is the doping concentration of the gap region, and V_{fb} is the flat band voltage. Under the assumption that there is no trap charge in the gate oxide, V_{fb} is equal to the difference in the work functions between M2 and Si (gap region), that is, $V_{fb=}\varphi_2 - \varphi_{Si}$, where φ_{Si} is the work function of Si, which can be calculated as follows:

$$\varphi_{Si} = \chi_{Si} + \frac{E_g}{2} - \frac{KT}{q}\ln\frac{N_{gap}}{n_i}, \tag{4}$$

where χ_{Si} is the electronic affinity of Si, and n_i expresses the intrinsic carrier concentration. E_g is the band gap of Si. K is the Boltzmann constant and T is the temperature. S If the impact of V_{ds} is neglected, the width of the depletion layer x_d in the gap region is:

$$x_d = \sqrt{\frac{2\varepsilon_{Si}|\varphi_s|}{qN_{gap}}}. \tag{5}$$

Figure 5(d) shows the calculated x_d and leakage current (I_{leak}) of the HMG LTFETs extracted from Fig. 5(b) at $V_{gs} = -0.1$ V. Based on the calculated results, the 3-nm-thick gap region was fully depleted when N_{gap} was less than 6×10^{19} cm^{-3}, and accordingly, I_{leak} was almost unchanged in this range. When N_{gap} increased, the channel of the JLT became partially depleted. The electrons could drift and diffuse at the bottom of this region, and the non-depleted region for electrons to flow broadened with increasing N_{gap}, which caused the I_{leak} to rise sharply. This dependence of the off-state performance on the channel doping concentration was observed in some previous researches concerning JLTs.[37–39] These results indicated that, to suppress the off-state leakage current, the gap-gate material and n-type doping level in the gap region should be simultaneously optimized to make the gap region fully depleted.

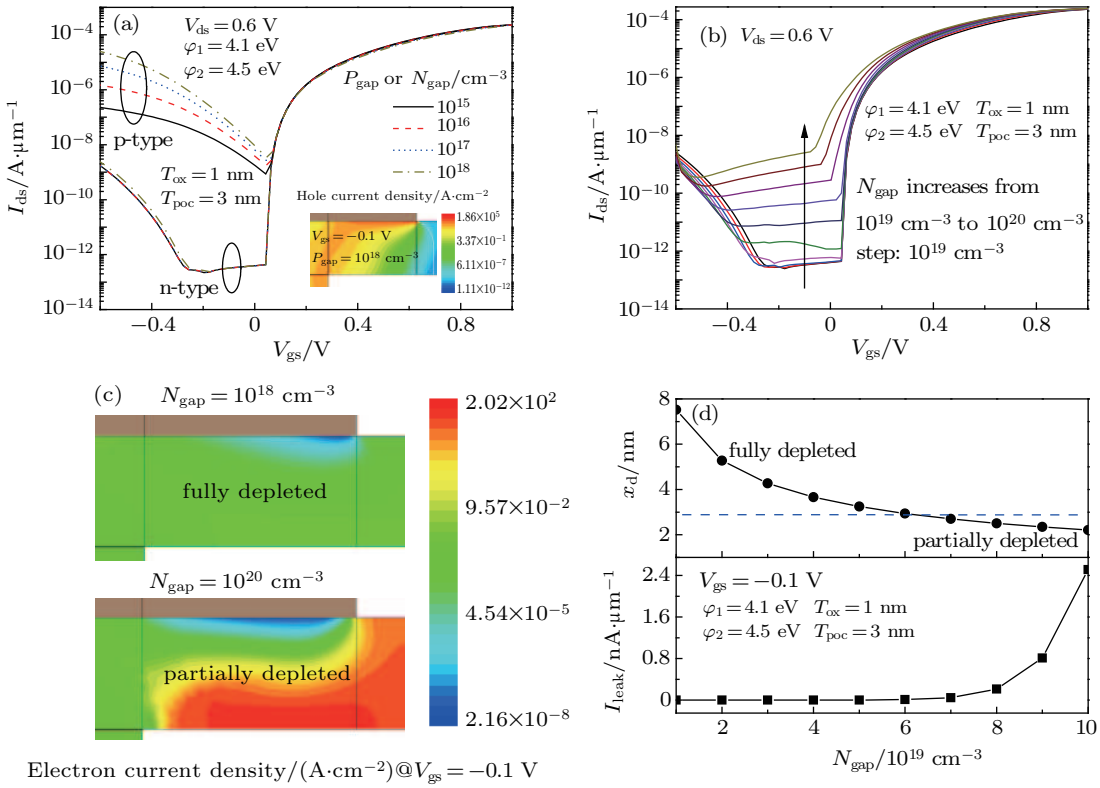

Fig. 5. (color online) (a) I_{ds}–V_{gs} characteristics of HMG LTFETs with various dopant types and doping concentrations in the gap. The n-type dopants endow the transistor with a flat window. (b) I_{ds}–V_{gs} characteristics of HMG LTFETs with an n-type gap with N_{gap} increasing from 10^{19} cm^{-3} to 10^{20} cm^{-3}. (c) Electron current density diagram in the lateral direction for HMG LTFETs with $N_{gap}=10^{18}$ cm^{-3} and 10^{20} cm^{-3}. (d) Calculated x_d and extracted I_{leak} for HMG LTFETs with n-type gap as functions of N_{gap}.

4. Conclusions

We proposed a symmetric HMG LTFET based on a Si/Ge heterojunction and demonstrated its properties through 2D numerical simulations. It was shown that the introduction of the gap gate with a work function different from that of the pocket gate significantly suppressed I_{off} and improved SS because of the lateral energy-band profile modulation. On this basis, the work function mismatch between the pocket gate and the gap gate, the dopant type, and the doping level in the gap region could all be tuned to enhance the performance. By optimizing the off-state leakage current and retaining the advantages of the high on-state current of the LTFETs, this proposed HMG LTFET could demonstrate potential for low-power applications.

References

[1] He J, Bian W, Tao Y D, Liu F, Song Y and Zhang X 2006 *Chin. Phys. Lett.* **23** 3373

[2] Theis T N and Solomon P M 2010 *Science* **327** 1600

[3] Choi W Y, Park B G, Lee J D and Liu T J K 2007 *IEEE Electron Device Lett.* **28** 743

[4] Verhulst A S, Leonelli D, Rooyackers R and Groeseneken G 2011 *J. Appl. Phys.* **110** 024510

[5] Wang P F, Lin X, Liu L, Sun Q Q, Zhou P, Liu X Y, Liu W, Gong Y and Zhang D W 2013 *Science* **341** 640

[6] Wang C, Wu C L, Wang J X, Huang Q Q and Huang R 2015 *Sci. China Inform. Sci.* **58** 022402

[7] Hähnel D, Oehme M, Sarlija M, Karmous A, Schmid M, Werner J, Kirfel O, Fischer I and Schulze J 2011 *Solid-State Electron.* **62** 132

[8] Zhou G, Lu Y, Li R, Zhang Q, Hwang W S, Liu Q, Vasen T, Chen C, Zhu H, Kuo J M, Koswatta S, Kosel T, Wistey M, Fay P, Seabaugh A and Xing H 2011 *IEEE Electron Device Lett.* **32** 1516

[9] Kao K H, Verhulst A S, Vandenberghe W G, Sorée B, Magnus W, Leonelli D, Groeseneken G and Meyer K D 2012 *IEEE Trans. Electron Devices* **59** 2070

[10] Ganapathi K and Salahuddin S 2011 *IEEE Electron Device Lett.* **32** 689

[11] Li R, Lu Y, Zhou G, Liu Q, Chae S D, Vasen T, Hwang W S, Zhang Q, Fay P, Kosel T, Wistey M, Xing H and Seabaugh A 2012 *IEEE Electron Device Lett.* **33** 363

[12] Jiang Z, Zhuang Y Q, Li C, Wang P and Liu Y Q 2016 *Chin. Phys. B* **25** 027701

[13] Walke A M, Verhulst A S, Vandooren A, Verreck D, Simoen E, Rao V R, Groeseneken G, Collaert N and Thean A V Y 2013 *IEEE Trans. Electron Devices* **60** 4057

[14] Mookerjea S, Mohata D, Krishnan R, Singh J, Vallett A, Ali A, Mayer T, Narayanan V, Schlom1 D, Liu A and Datta S 2009 *IEEE International Electron Device Meeting*, December 7–9, 2009, Baltimore, MD, United States, p. 13.7.1

[15] Liu Y, Wang H J, Yan J and Han G Q 2013 *Chin. Phys. Lett.* **30** 088502

[16] Kazazis D, Jannaty P, Zaslavsky A, Royer C L, Tabone C, Clavelier L and Cristoloveanu S 2009 *Appl. Phys. Lett.* **94** 263508

[17] Qiu Y X, Wang R S, Huang Q Q and Huang R 2014 *J. Appl. Phys.* **115** 234505

[18] Kim S H, Kam H, Hu C and Liu T J K 2009 *Symposium on VLSI Technology*, June 16–18, 2009, Kyoto, Japan, p. 178

[19] Liu Y, He J, Chan M, Du C X, Ye Y, Zhao W, Wu W, Deng W L and Wang W P 2014 *Chin. Phys. B* **23** 097102

[20] Zhan Z, Huang Q Q, Huang R, Jiang W Z and Wang Y Y 2013 *Science China Information Science* **56** 072401

[21] Huang R, Huang Q Q, Chen S W, Wu C L, Wang J X, An X and Wang Y Y 2014 *Nanotechnology* **25** 505201

[22] Fischer I A, Bakibillah A S M, Golve M, Hähnel D, Isemann H, Kottantharayil A, Oehme M and Schulze J 2013 *IEEE Electron Device Lett.* **34** 154

[23] Blaeser S, Glass S, Schulte-Braucks C, Narimani K, Driesch N, Wirths S, Tiedemann A T, Trellenkamp S, Buca D, Zhao Q T and Mantl S 2015 *IEEE International Electron Devices Meeting*, Decemeber 7–9, 2015, Washington, USA, p. 22.3.1

[24] Brouzet V, Salem B, Periwal P, Alcotte R, Chouchane F, Bassani F, Baron T and Ghibaudo G 2016 *Solid-State Electron.* **118** 26

[25] Zhao Q T, Richter S, Schulte-Braucks C, Knoll L, Blaeser S, Luong G V, Trellenkamp S, Schafer A, Tiedemann A, Hartmann J M, Bourdelle K and Mantl S 2015 *IEEE J. Electron Devices Soc.* **3** 103

[26] Kim M, Wakabayashi Y K, Yokoyama M, Nakane R, Takenaka M and Takagi S 2015 *IEEE Trans. Electron Devices* **62** 9

[27] Ghosh S, Koley K, Saha S K and Sarkar 2016 *IEEE Trans. Electron Devices* **63** 3869

[28] Zhou G, Li R, Vasen T, Qi M, Chae S, Lu Y, Zhang Q, Zhu H, Kuo J M, Kosel T, Wistey M, Fay P, Seabaugh A and Xing H 2012 *IEEE International Electron Devices Meeting*, December 10–13, 2012 San Francisco, CA, USA, p. 32.6.1

[29] Bhuwalka K K, Sedlmaier S, Ludsteck A K, Tolksdorf C, Schulze J and Eisele I 2004 *IEEE Electron Device Lett.* **51** 279

[30] Zhou G, Lu Y, Li R, Zhang Q, Hwang W S, Liu Q, Vasen T, Chen C, Zhu H, Kuo J M, Kosel T, Wistey M, Fay P, Seabaugh A and Xing H 2012 *IEEE Electron Device Lett.* **33** 782

[31] Cui N, Liang R and Xu J 2011 *Appl. Phys. Lett.* **98** 142105

[32] Saurabh S and Kumar M J 2011 *IEEE Trans. Electron Devices* **58** 404

[33] Sentaurus device user guide. 2013 Version Y-2013.03

[34] Colinge J P, Lee C W, Afzalian A, Akhavan N D, Yan R, Ferain I, Razavi P, O'Neill B, Blake A, White M, Kelleher A M, McCarthy B and Murphy R 2010 *Nat. Nanotechnol.* **5** 225

[35] Kim S H, Agarwal S, Jacobson Z A, Matheu P, Hu C and Liu T J K 2010 *IEEE Electron Device Lett.* **31** 1107

[36] Schlosser M, Bhuwalka K K, Sauter M, Zibauer T, Sulima T and Eisele I 2009 *IEEE Trans. Electron Devices* **56** 100

[37] Sun C, Liang R, Liu L, Wang J and Xu J 2015 *Appl. Phys. Lett.* **107** 132105

[38] Lee C W, Ferain I, Afzalian A, Yan R, Akhavan N D, Razavi P and Colinge J P 2010 *Solid-State Electron.* **54** 97

[39] Choi S J, Moon D I, Kim S, Duarte J P and Choi Y K 2010 *IEEE Electron Device Lett.* **32** 152